

Synthesis and characterization of metal doped molecular sieve 5Å-based catalyst

L. Kumar¹, A. G. Chakinala², M. G. H. Zaidi³, P. Kumar^{1*}

¹Department of Physics, Manipal University Jaipur, Jaipur-303007, Rajasthan, India

²Department of Biotechnology and Chemical Engineering, Manipal University Jaipur, Jaipur-303007, Rajasthan, India

³Department of Chemistry, College of Basic Science and Humanities, G.B Pant University of Agriculture and Technology, Uttarakhand, 263145, India

Received: March 20, 2023; Revised: April 30, 2023

Conversion of waste to best in the form of valuable product using different catalysts is the need of present time for an emerging technological application. However, achieving the appropriate yield of best with negligible waste generation at low energy consumption is still a grand challenge. In the process of converting waste to best the catalyst plays an important role for green chemistry. In this report, we have synthesized metal, i.e., zinc- and iron-doped molecular sieve 5Å catalyst using chemical synthesis process. The synthesized catalyst was identified by diverse analytical techniques. Optical spectra revealed the reduction in band gap of metal-doped molecular sieve by 5Å, which was attributed to localized state formation within the band gap of base material molecular sieve 5Å. Such materials can find technological applications in green chemistry to convert waste into valuable chemicals.

Keywords: Molecular sieve 5Å, Metal doping, Chemical synthesis, FESEM.

INTRODUCTION

Nanotechnology's progress has sparked a surge of fascination in transition metal catalysts due to their versatile applications. These catalysts, composed of transition metals, find extensive use in various fields such as wastewater treatment, rechargeable batteries, and catalytic hydrogenation [1]. The use of transition metals, such as iron and zinc, offers several benefits, including being cost-effective and readily available in nature [2]. In recent years, the discharge of pollutants into water environments has emerged as a critical concern, endangering both human health and aquatic ecosystems. To combat this issue, extensive research has been conducted to develop metal nanoparticles as efficient catalysts for the elimination of these harmful contaminants [3]. The incorporation of metallic and acidic sites within a unified nanocomposite material has been the subject of extensive research in catalytic applications for many years. The exceptional thermal stability, acidity, and distinctive nanoscale porous structure of molecular sieve 5Å (MS-5Å) have positioned it as a promising candidate for introducing acidic functionality. Various catalytic reactions have demonstrated the exceptional efficiency of composite materials combining metals and molecular sieve 5Å in catalysis [4].

The porous structure of molecular sieve 5Å has rendered it a promising candidate for hosting the synthesis of nanoparticles. These materials can be obtained through natural processes or laboratory techniques and typically comprise alumina (Al₂O₃),

silica (SiO₂), alkali or alkaline-earth metals, as well as water molecules trapped inside the pores [5]. The molecular sieve 5Å exhibits a regular microsphere structure in one-, two-, and three-dimensions, resulting in an extensive network of cages and channels with precise shapes and sizes [6]. In this context, Xu *et al.* conducted a comprehensive assessment on the summary of metal nanoparticle catalysts [7]. Additionally, David *et al.* provided insights into the perspectives and applications of molecular sieve 5Å containing metal nanoparticles in catalysis [8]. Wu *et al.* investigated the confinement of noble nanometals within a molecular sieve 5Å matrix, highlighting the notable advantages in size and site adjustment, as well as nano-architecture model.

Recently, the scientific community has extensively investigated the influence of transition metal catalysts on catalytic capabilities. However, there is a notable absence of studies exploring the synthesis of Zn and Fe-doped MS-5Å composite nanomaterials. This knowledge gap in the literature motivated the scope of the present work. Building upon our interest in synthesizing new nanostructured compounds with applications in metal-organic framework synthesis and wastewater treatment [9, 10], we present a simple chemical synthesis process for making zinc and iron-doped MS-5Å materials. The synthesized samples were analyzed using XRD, FTIR spectroscopy, FESEM, and UV-Vis techniques. The synthesis of nanosized catalysts within the molecular sieve 5Å framework represents an innovative approach towards achieving efficient

* To whom all correspondence should be sent:

E mail: pushpendra.kumar@jaipur.manipal.edu

catalytic reactions. These MS-5Å-based nanocomposites hold potential for various multifunctional applications, which will be the focus of our future endeavors.

EXPERIMENTAL

Material

For this research work, reagents: urea ($\text{CH}_4\text{N}_2\text{O}$), iron (III) nitrate nonahydrate ($\text{Fe}(\text{NO}_3)_3 \cdot 9\text{H}_2\text{O}$) and zinc nitrate hexahydrate ($\text{Zn}(\text{NO}_3)_2 \cdot 6\text{H}_2\text{O}$) were used without any purification. Molecular sieve-5Å was purchased from Gujrat Multi Gas Base Chemicals Pvt. Ltd. Ethanol was used for the synthesis.

Sample preparation

A straightforward chemical synthesis method was employed to fabricate composite nanostructures (CNs) of iron and zinc-doped molecular sieve 5Å (MS-5Å). At first, finely crushed MS-5Å (3 g) was added to ethanol (15 mL), followed by the addition of urea (1.5 g) dissolved in ethanol (15 mL). The resulting pinkish product was stirred for 1 hour. Subsequently, iron (III) nitrate nonahydrate ($\text{Fe}(\text{NO}_3)_3 \cdot 9\text{H}_2\text{O}$) and zinc nitrate hexahydrate ($\text{Zn}(\text{NO}_3)_2 \cdot 6\text{H}_2\text{O}$) solutions (1.6 g each) were slowly dropwise mixed into the solution while continuously stirring at 60°C for 2 hours. The resulting mixture was then sonicated for 1 hour, filtered, and dried overnight at room temperature. Finally, the dried samples (Zn/MS-5Å and Fe/MS-5Å) were calcined at 500°C for 5 hours and placed in a desiccator. In total, there were three samples - molecular sieve-5 Å named as sample S1, Zn-doped MS-5Å named as sample S2 and Fe-doped MS-5Å named as sample S3.

Characterization

The synthesized catalyst underwent comprehensive characterization using various methods to analyze its structural, morphological, functional, and optical properties. The UV-Vis spectra were recorded in absorbance mode on a Shimadzu UV-NIR 2600, Japan instrument in the range of 190-800 nm at ambient temperature. Prior to measurement, the synthesized samples were dissolved in deionized (DI) water and subjected to sonication for approximately 1 hour. The obtained absorbance data were utilized to evaluate the energy gap (E_g) of both samples by constructing Tauc plots that correlate energy with the square of the absorption coefficient $(\alpha h\nu)^2$. The structural analysis

of the prepared materials showed various functional groups, using a Fourier transform infrared (FTIR) spectrometer model Bruker Alpha from the USA. The spectra were documented in the scale of 500-4000 cm^{-1} .

The structural characterization was made using a programmed multipurpose X-ray diffractometer (model: SMARTLAB) manufactured by Rigaku. The instrument employed a wavelength of Cu K α radiation of 0.15406 nm. The detector was operated at a voltage of 40 kV with a filament current of 30 mA. The XRD patterns were recorded for all samples in the span of $10^\circ \leq 2\theta \leq 80^\circ$, with a scanning rate of 0.02 θ /s at room temperature. This analysis aimed to investigate the size, phase and crystal structure of the prepared materials. The morphology, shape, and size of the synthesized samples were analyzed using a field effect scanning electron microscope (FESEM) model JEOL-7610F, Japan. Additionally, the elemental constituents of the samples were analyzed by energy dispersive X-ray spectroscopy (EDX), which was integrated with the same FESEM instrument.

RESULTS AND DISCUSSION

Structural study

The XRD patterns of the prepared material are illustrated in Fig. 1. The XRD patterns exhibit multiple peaks, indicating the crystalline nature of the compounds. The diffraction peaks, observed at specific 2θ values, correspond to various crystallographic planes. Specifically, the peaks located at approximately 6.30°, 10.20°, 11.94°, 15.69°, 18.67°, 20.32°, 23.57°, 26.93°, 30.60°, 31.25°, 32.29°, and 33.90° can be indexed to the (200), (220), (311), (331), (511), (440), (533), (642), (660), (751), (840), and (664) planes, respectively, which are associated with the molecular sieve 5 Å present in our samples. The observed diffraction peaks closely correspond to the characteristic peaks of the alumina and silica tetrahedral framework. Notably, the dominant peak (200) is observed at an approximate 2θ value of 6.30° [11]. To determine the crystallite size (t_{DS}) of the sample for the respective crystal plane orientations, the Debye-Scherrer formula was employed [12]:

$$t_{DS} = \frac{k\lambda}{\beta_{hkl} \cos\theta_{hkl}} \quad (1)$$

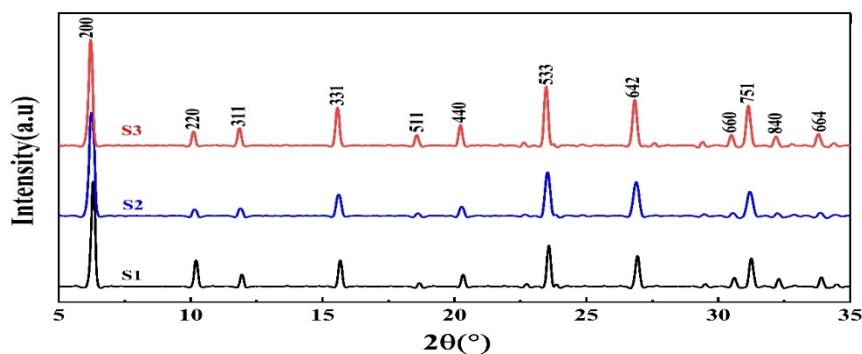


Fig. 1. XRD spectra of MS-5Å (S1), Zn/MS5Å (S2) and Fe/MS5Å (S3)

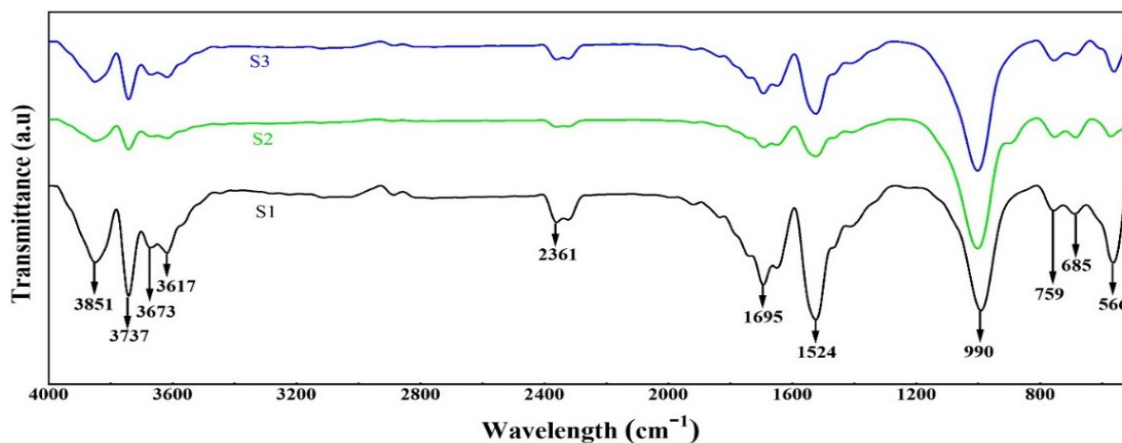


Fig. 2. FTIR spectra of samples S1, S2, and S3.

The determined values of crystallite size for samples S1, S2, and S3 are 53.38 nm, 54.02 nm, and 56.23 nm, respectively. It is noted that the crystallite size of samples S2 and S3 is larger compared to sample S1. This increase in crystallite size can be attributed to the heating treatment that samples S2 and S3 underwent during the synthesis process. The supplied heat energy during calcination facilitates the diffusion and rearrangement of atoms or molecules within the sample, leading to the agglomeration and growth of existing crystallites. This phenomenon, known as crystallite growth or crystallite coarsening, causes the average crystallite size to increase after calcination.

FTIR study

The different groups contained in the materials were examined by FTIR. Figure 2 illustrates the FTIR spectra of MS-5Å, Zn/MS-5Å, and Fe/MS-5Å composite nanomaterials (CNs) in the measurable range of 500 to 4000 cm^{-1} . The wave number corresponding to 566 cm^{-1} was attributed to the bending vibrations of the T-O (T = Al, Si groups) in

the sieve [13, 14]. These peaks also represent the bending vibration of the internal tetrahedron TO_4 of the MS-5Å structure, indicating the existence of Al^{3+} and Si^{4+} in the sieve. The peak at 685 cm^{-1} is associated with Si-O-Si, while the peak at 759 cm^{-1} corresponds to the symmetrical stretching (T-O-T, T = Si, Al) [15]. The band near 990 cm^{-1} is related to the symmetric vibrations of Si-O (bridging) and Si-O- (non-bridging) bonds [16]. The bands detected at 1524 and 1695 cm^{-1} are related to the OH bending vibration of water molecules [17]. The band at 2361 cm^{-1} may be attributed to the interaction between Zn/MS-5Å, Fe/MS-5Å, and TO_4 in the sieve during the doping process [18, 19]. The samples exhibit distinctive bands corresponding to AlO-H groups (at 3737 and 3673 cm^{-1}), Si-OH-Al acidic hydroxyls (at 3617 cm^{-1}) [20, 21], and external SiO-H groups (at 3851 cm^{-1}) (Figure 2), consistent with previous studies [22]. The introduction of metal ions into the molecular sieve directs to a significant decrease in the intensity of these bands (Figure 2), indicating that the zinc and iron species interact with several hydroxyl groups of the pristine support.

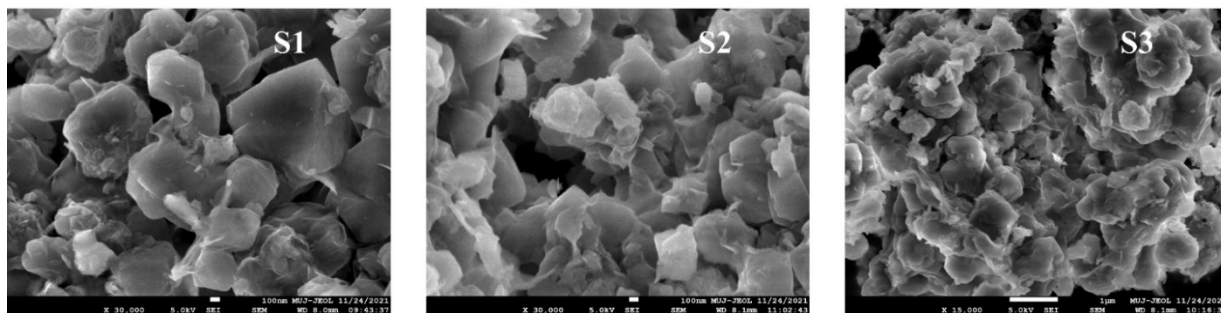


Fig. 3. FESEM images of the samples S1, S2 and S3

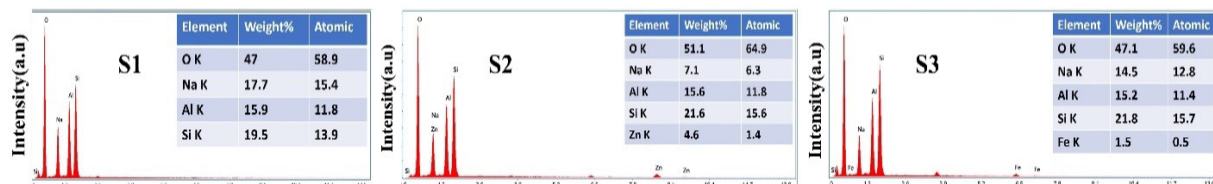


Fig. 4. XEDS spectra of the samples S1, S2 and S3.

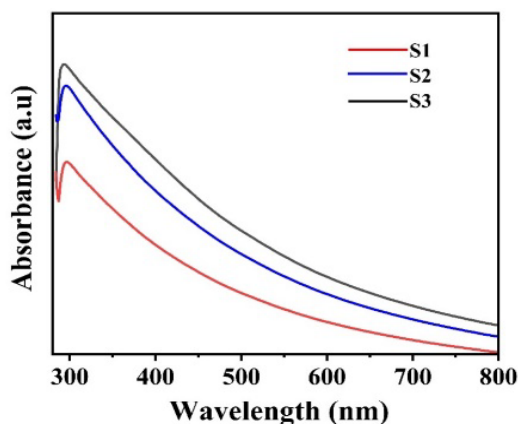


Fig. 5. Absorbance spectra of the samples S1, S2 and S3

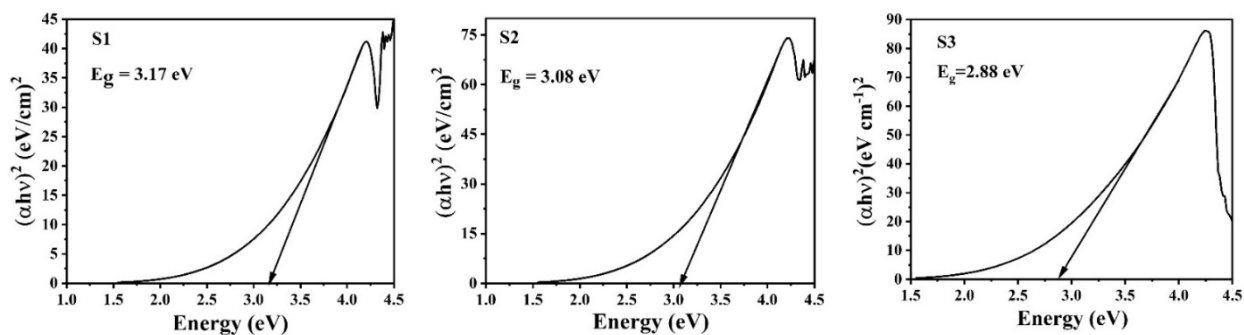


Fig. 6. Tauc plots of the samples S1, S2 and S3

Microstructural studies

FESEM analysis

The morphology of the samples was studied using high-resolution FESEM. The images exhibit that the mean diameter of the samples ranged from 100 nm to 1 μm and were aggregated in shape with a high density, as seen in Fig. 3. The findings suggest that the blending methodology used resulted in well-

formed Zn/MS-5Å and Fe/MS-5Å, as supported by previous studies [23, 24]. The results showed that the samples consisted of oxygen, iron, silicon, zinc, and aluminum, as seen in Fig. 4. The data from the selected area analysis by XEDS, which included a comparative elemental analysis, confirmed that the Zn/MS-5Å and Fe/MS-5Å are composed of the elements and no impurities were detected. The obtained Zn and Fe content agreed with the

theoretical zinc and iron content in the Zn/MS-5Å and Fe/MS-5Å, as seen in Fig. 4 [25].

Optical behavior

The optical study of the samples was performed in the wavelength scale of 190-800 nm, as depicted in Figure 5. The Tauc plots, based on the relation involving the absorption coefficient and the energy of the incident light, are shown in Figure 6. These plots were utilized to estimate the band gap energy [26-29].

$$(\alpha h\nu) = \beta (h\nu - E_g)^r \text{ for } h\nu > E_g \quad (2)$$

and

$$(\alpha h\nu) = 0 \text{ for } h\nu < E_g \quad (3)$$

where, absorption coefficient (α) was evaluated using absorbance (A) by the formula $\alpha = (2.303 * A / x)$, where x represents the width of the sample. A constant β was introduced, and the optical energy gap (E_g) was determined using a linear fit of the experimental data. The parameter r can take values of 1/2 and 2 for direct and indirect admitted transitions, respectively, which depends on the nature of electron transitions accountable for the optical absorption. Based on the linear fits, the band gap values for samples S1, S2, and S3 were evaluated to be around 3.177 eV, 3.08 eV, and 2.88 eV. It is observed that the band gap decreases with metal doping. This drop in band gap can be related to the increase in crystallite size, as evidenced by the XRD analysis.

CONCLUSION

In this study the synthesis of metal-supported MS-5Å nanoparticles was performed using a chemical method. The effect of heating during sample synthesis was evaluated in terms of its impact on crystallite size and optical properties. The results revealed that the increased agglomeration in the synthesized nanomaterials, due to heating, was the primary reason for the observed changes. The band gap of the sample showed a significant shift, from 3.17 eV in sample S1 to 3.08 eV in S2 and 2.88eV in S3, because of the alterations in structural parameters and crystallite size caused by the agglomeration. These findings demonstrate the feasibility of modulating the properties of molecular sieves 5Å through variations in synthesis parameters and doping with different transition metals. This study contributes to the advancement of knowledge in the field by providing insights into the behavior of the synthesis process of different molecular sieves and its potential applications in industries such as biomedical, wastewater treatment, and thermochemical heat storage.

REFERENCES

1. G. Allaedini, S. M. Tasirin, P. Aminayi, *Chemical papers*, **70**, 231 (2016).
2. X Du, H Su, X Zhang, *Journal of Catalysis*, **383**, 103 (2020).
3. A. Karbul, M. K. Mohammadi, R. J. Yengejeh, F. Farrokhian, *Material Research*, **24**, e20200292 (2021).
4. E Nyankson, J. Adjasoo, J. K. Efavi, A Yaya, G. Manu, A. Kingsford, R. Y. Abrokwah, *Scientific African*, **7**, e00257 (2020).
5. M. Yoldi, E.G.Fuentes-Ordoñez, S.A.Korili, A.Gil, *Powder Technology*, **366**,175 (2020).
6. H. Jahangirian, R. Moghaddam, N. Jahangirian, B. Nikpey, S. Jahangirian, N. Bassous, B. Saleh, K. Kalantari, T. J. Webster, *Int. J Nanomedicine*, **15**, 1005 (2020).
7. D. Xu, H. Lv, B. Liu, *Frontiers in Chemistry*, **6**, (2018).
8. D. Farrusseng, A. Tuel, *New Journal of Chemistry*, **40**,3933 (2016).
9. M. K. Mohammadi, A. Gutiérrez, P. Hayati, K. Mohammadi, R. Rezaei, *Polyhedron*, **160**, 20 (2019).
10. A. Derakhshan-Nejad, H. A. Rangkooy, M. Cheraghi, R. J. Yengejeh, *J Environ. Health Sci, Eng.*, **18**, 201 (2020).
11. R. M. Barrer, P. J. Denny, *J. Chem. Soc.*, **0**, 971 (1961).
12. Harish, P. Kumar, J. Kumari, P. Phalasal, P. K. Khanna, A. Salim, R. Singhal, A. K. Mukhopadhyay, R. P. Joshi, *Journal of Nano- and Electronic Physics*, **13**, 01029 (2018).
13. B. Kwakye-Awuah, E.Von-Kiti, I. Nkrumah, R. Erdoolkyreve, I. Radecka, C. Williams, *Desalin.. Water Treat.*, **57**, 21654 (2016).
14. A. Zainal Abidin, Abu Bakar NHH, Ng. EP, W. Tan, *J. Taibah Univ. Sci.*, **11**,1070 (2017).
15. H. L. Wang, J. Y. Cui, W. F. Jiang, *Mater. Chem. Phys.*, **130**, 993 (2011).
16. B. Kwakye-Awuah, D. D. Wemegah, I. Nkrumah, C. Williams, I. Radecka, *Int J, Sci Res.*, **2**, 26 (2013).
17. M. S. Boroglu, M. A. Gurkaynak, *Polym Bull.*, **66**,463 (2011).
18. X.Guo, A. Navrotsky, *Microporous Mesoporous Mater.*, **268**, 197 (2018).
19. A. Asiedu, S. Kumar, *Ind. Eng. Chem. Res.*, **58**, 15787 (2019).
20. E. Bourgeat-Lami, F. Fajula, D. Anglerat, T. Des Courieres, *Microporous Mater.*, **1**, 237 (1993).
21. A. Janin, M. Maache, J. C. Lavalley, J. F. Joly, F. Raatz, N. Szydlowski, *Zeolites.*, **11**, 391 (1991).
22. A. Jentys, N. H. Pham, H. J Vinek, *Chem. Soc. Faraday Trans.*, **92**, 3287 (1996)
23. X. Zhang, Q. Shen, C. He, C. Ma, J. Cheng, Z. Liu Z. Hao, *Catal. Sci. Technol.*, **2**, 1249 (2012).
24. E. F. Iliopoulou, S. Stefanidis, K. Kalogiannis, A. C. Psarras, A. Delimitis, K. S. Triantafyllidis, A. A. Lappas, *Green Chem.*, **16**, 662 (2014).
25. Y. Ding, Y. Wang, L. Zhang, H. Zhang, C. M. Li Y. Lei, *Nanoscale*, **3**, 1149 (2011).

26. P. Kumar, P. Lemmens, *RSC Adv.*, **5**, 91134 (2015).
27. Harish, P. Kumar, V. Kumar, R. K. Mishra, J. S. Gwag, M. K. Singh, R. Singhal, A. K. Mukhopadhyay, *Ceramic International*, **48**, 35771 (2022).
28. Harish, P. Kumar, S. Kumari, M. Debnath, A. Salim, R. Singhal, R. P. Joshi, and A. K. Mukhopadhyay, *Journal of Material Science*, **57**, 8241 (2022).
29. Akash, Harish, J. Kumari, A. K. Mukhopadhyay, P. Kumar, *Chemistry Select.*, **7**, e202200417 (2022).